Femtosecond Polarization Shaping of Free-Electron Laser Pulses

Giovanni Perosa et al.

Phys. Rev. Lett. **131**, 045001 — Published 24 July 2023

DOI: 10.1103/PhysRevLett.131.045001

Femtosecond polarization shaping of free-electron laser pulses

Giovanni Perosa,[1,2] Jonas Wätzel,[3] David Garzella,[1] Enrico Allaria,[1] Matteo Bonanomi,[4,5] Miltcho Boyanov Danailov,[1] Alexander Brynes,[1] Carlo Callegari,[1] Giovanni De Ninno,[1,6] Alexander Demidovich,[1] Michele Di Fraia,[1,7] Simone Di Mitri,[1,2] Luca Giannessi,[1,8] Michele Manfredda,[1] Luka Novinec,[1] Nitish Pal,[1] Giuseppe Penco,[1] Oksana Plekan,[1] Kevin C. Prince,[1] Alberto Simoncig,[1] Simone Spampinati,[1] Carlo Spezzani,[1] Marco Zangrando,[1,7] Jamal Berakdar,[3] Raimund Feifel,[9] Richard J. Squibb,[9] Ryan Coffee,[10] Erik Hemsing,[10] Eléonore Roussel,[11] Giuseppe Sansone,[12] Brian W. J. McNeil,[13,14,15] and Primož Rebernik Ribič[1,*]

[1] *Elettra-Sincrotrone Trieste, 34149 Basovizza, Trieste, Italy*
[2] *Department of Physics, Università degli Studi di Trieste, 34127 Trieste, Italy*
[3] *Institut für Physik, Martin-Luther-Universität Halle-Wittenberg, 06099 Halle (Saale), Germany*
[4] *Politecnico di Milano, 20133 Milano, Italy*
[5] *Istituto di Fotonica e Nanotecnologie, 20133 Milano, Italy*
[6] *Laboratory of Quantum Optics, University of Nova Gorica, 5001 Nova Gorica, Slovenia*
[7] *Istituto Officina dei Materiali, Consiglio Nazionale delle Ricerche, 34149 Basovizza, Italy*
[8] *ENEA C.R. Frascati, 00044 Frascati (Roma), Italy*
[9] *Department of Physics, University of Gothenburg, 41133 Gothenburg, Sweden*
[10] *SLAC National Accelerator Laboratory, Menlo Park, California 94025, USA*
[11] *Univ. Lille, CNRS, UMR 8523 - PhLAM - Physique des Lasers Atomes et Molécules, F-59000 Lille, France*
[12] *Physikalisches Institut, Albert-Ludwigs-Universität Freiburg, 79085 Freiburg, Germany*
[13] *University of Strathclyde (SUPA), Glasgow G4 0NG, United Kingdom*
[14] *Cockcroft Institute, Warrington, WA4 4AD, United Kingdom*
[15] *ASTeC, STFC Daresbury Laboratory, Warrington, WA4 4AD, United Kingdom*

(Dated: 14th June 2023)

We demonstrate the generation of extreme-ultraviolet (XUV) free-electron laser (FEL) pulses with time-dependent polarization. To achieve polarization modulation on a femtosecond time scale, we combine two mutually delayed counter-rotating circularly polarized sub-pulses from two cross-polarized undulators. The polarization profile of the pulses is probed by angle-resolved photoemission and above-threshold ionization of helium; the results agree with solutions of the time-dependent Schrödinger equation. The stability limit of the scheme is mainly set by electron-beam energy fluctuations, however, at a level that will not compromise experiments in the XUV. Our results demonstrate the potential to improve the resolution and element selectivity of methods based on polarization shaping and may lead to the development of new coherent control schemes for probing and manipulating core electrons in matter.

Generation of laser pulses whose polarization is modulated on a femtosecond time scale is an established technique in the visible spectrum [1, 2]. It has been used in a number of applications, e.g., as an optical centrifuge for rotational acceleration [3] and controlled orientation of molecules [4], to maximize the photoionization yield of diatomic molecules [5, 6], for coherent control of electron wavepackets [7–9], to produce attosecond pulses [10, 11], and many others [12–14]. The same ability in the extreme-ultraviolet (XUV) and x-ray spectral regions would improve resolution and element selectivity, and potentially lead to the development of new coherent control methods for probing and manipulating core electrons and associated phenomena.

In the visible, a time-dependent polarization of a laser pulse is accomplished using a pulse shaper [15–17]. Lack of efficient optical elements and greater difficulties in controlling the propagation of light at short wavelengths significantly restrain pulse shaping in the XUV/x-ray spectral region. Pulse shapers are practically impossible to fabricate and the only viable options are *in situ* (*i.e.*, during the light generation process itself) techniques. We show here that harmonic conversion of a coherent pulse to shorter wavelengths using the externally seeded free-electron laser (FEL) FERMI [18] provides a solution to the problem of tailoring the polarization profile of short and intense XUV/x-ray pulses. Seeded FELs are among the newest light sources and generate fully coherent femtosecond pulses of short wavelength light with tunable properties [19–25]. Because they are accelerator based, the methods for controlling their output may be very different from those of conventional lasers, and here we demonstrate an important application.

With a seeded FEL, polarization control can be achieved by generating two mutually delayed, phase-locked, cross-polarized FEL sub-pulses (counter-rotating circular polarizations, or perpendicular linear polarizations) [26–28]. Only the zero-delay case has already been demonstrated at FERMI [29, 30]; the finite-delay case, which is essential to a time-varying polarization, has not yet been demonstrated at any FEL.

The proposed and experimentally demonstrated layout is sketched in Fig. 1. After interacting with the seed

* primoz.rebernik@elettra.eu

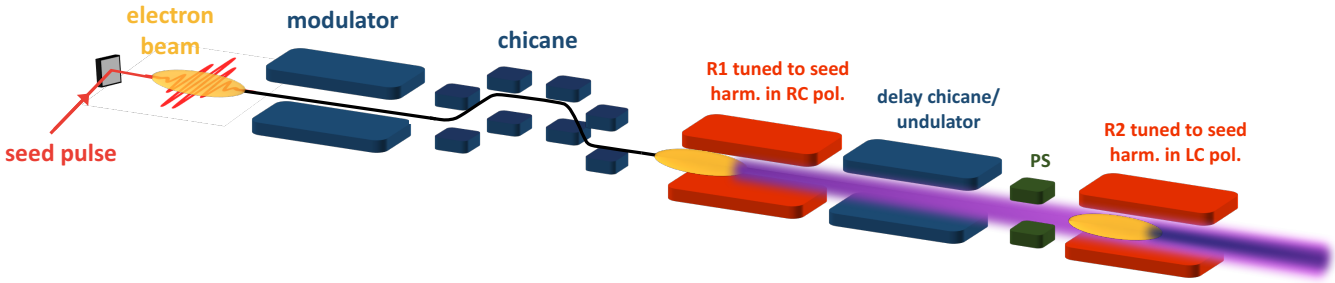

Figure 1: The scheme for generating an XUV FEL pulse with time-dependent polarization. See text for details.

laser in the modulator and traversing a magnetic chicane, just as in any standard high-gain harmonic generation (HGHG) FEL [31], the microbunched portion of the electron beam emits a right-circularly (RC) polarized FEL pulse at an integer harmonic of the seed frequency in the downstream radiator R1. The electron beam is then delayed with respect to this FEL pulse using a highly dispersive element (delay chicane or undulator tuned to a non-integer harmonic of the seed) [32]. It then traverses R2, generating a left-circularly (LC) polarized FEL pulse. A phase shifter PS (a small chicane) located just before R2 is used to fine tune the relative phase between the two cross-polarized FEL sub-pulses. Two linearly polarized sub-pulses with orthogonal polarizations are equally possible, thanks to the variable-polarization design of the radiators [29].

The calculated properties of the output pulse are shown in Fig. 2 for two identical, cross-polarized sub-pulses with Gaussian envelopes separated in time by one full width half maximum (FWHM = 60 fs) and a relative phase of $\pi/4$. The left panel shows the on-axis x and y components of the total electric field E_x, E_y and the total intensity I. We analyze the pulses in terms of their Stokes parameters, normalized to $S_0 = I$: unlike pulses with time-independent polarization (e.g., pure circular), ours have time-dependent Stokes parameters, which are in general all different from zero. For the case in Fig. 2, the polarization evolves from RC in the pulse head ($t < -50$ fs), to linear in the pulse center ($t = 0$), to LC in the pulse tail ($t > 50$ fs).

Modifying the relative phase between the sub-pulses controls the Stokes parameters of the composite pulse, in particular the direction of the (purely linear) polarization at $t = 0$; the latter rotates in the polarization plane as the phase is varied. However, this also means that any unwanted shot-to-shot phase fluctuations will lead to a fluctuating output polarization, which may prevent the realization of the proposed scheme. In an FEL, such fluctuations are a consequence of electron-beam energy fluctuations (due to fluctuating radio frequency fields used to accelerate the beam), which are converted into trajectory fluctuations when the electrons propagate through dispersive sections of the FEL line. Even if the dispersion is set to zero, we expect residual phase fluctuations between the sub-pulses due to electron-beam trajectory

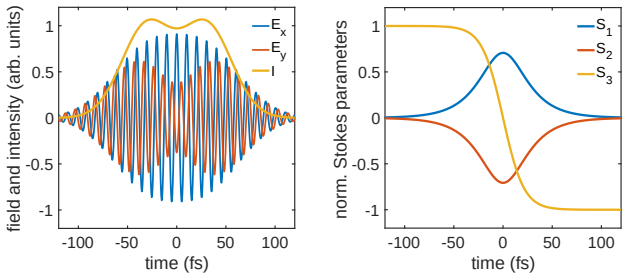

Figure 2: Schematic output of the setup shown in Fig. 1 for a separation between the sub-pulse envelopes equal to their FWHM durations (60 fs) and a relative phase of $\pi/4$. Left: components of the total electric field and total intensity. The FEL wavelength is exaggerated to visualize oscillations of the fields. Right: temporal profiles of the normalized Stokes parameters.

jitter along the FEL line.

To characterize the phase fluctuations, we first operated FERMI [18] at the sixth harmonic of a 250 nm seed ($\lambda_{FEL} \approx 42$ nm) in a co-rotating configuration with R1 (two radiator modules) and R2 (one module) both tuned to RC polarization [33] and measured the output intensity as a function of the relative phase between the sub-pulses. The sub-pulse duration estimated from the seed duration (120 fs) was 60 fs [19, 34]. The measurements were performed with balanced peak electric fields of the sub-pulses and sampling the FEL beam on axis through a 2.5 mm × 2.5 mm aperture located ∼ 50 m downstream of R2 to limit effects due to wavefront curvature.

Fig. 3, top shows the normalized intensity $2I/(I_{min} + I_{max})$ as a function of the phase added by PS for zero (left) and 30 fs (right) delay between the sub-pulse envelopes [36]. For zero delay, we observe a maximum (minimum) at $\sim 0.2\lambda$ ($\sim 0.7\lambda$), corresponding to constructive (destructive) interference between the sub-pulses [35]. From a simple model using two Gaussian pulses whose sources are separated in space (10 m separation, 100 μm source sizes) and time, the expected contrast (difference between the maximum and minimum signal) is higher (red curve). However, including a typical electron-beam trajectory jitter along the FEL line [37], the experiment

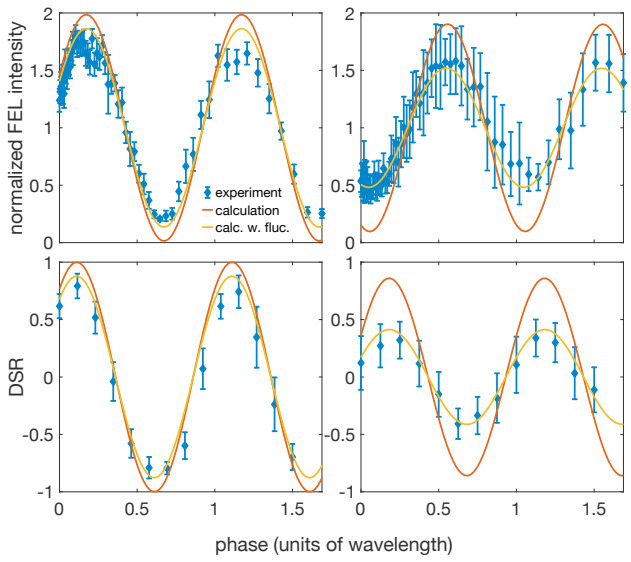

Figure 3: FEL intensity for co-rotating sub-pulses (top) and DSR obtained from decomposition of VMI images for counter-rotating sub-pulses (bottom) as a function of additional phase (generated by PS before R2 in Fig. 1) for zero (left) and 30 fs (right) delay between the sub-pulse envelopes. Error bars indicate ± one standard deviation calculated from (top) 50 measurements and (bottom) 1650 measurements (averaging performed over 2 FEL shots). Note that the absolute zero of the phase setting is not known [35].

agrees well with the model (yellow curve). Delaying the pulses by 0.5×FWHM of the sub-pulse duration, the experimental contrast is further reduced, partly because the overlap region where interference occurs is now shorter, but mostly due to additional phase fluctuations introduced by the undulator that delays the sub-pulses (note the larger error bars). In this case, the theoretical prediction matches the measurements after including relative electron-beam energy fluctuations on the order of 4×10^{-4}, corresponding well to the measured values at FERMI. The agreement between theory and experiment in the top panels of Fig. 3 also demonstrates that other fluctuations which might decrease the contrast (such as, e.g., relative intensity variations between the sub-pulses) are very small.

The root-mean-square phase fluctuations in Fig. 3 correspond to $\approx 0.06\lambda$ and $\approx 0.17\lambda$, for zero and 30 fs delay, respectively, and are therefore not expected to compromise the proposed scheme (they are smaller than $\lambda/4$). This is further demonstrated for counter-rotating fields (producing the output in Fig. 2) by tuning R2 to LC polarization. In this case, the FEL intensity does not depend on the relative phase. We therefore evaluated the fluctuations by measuring photoelectron distributions from He atoms excited by such FEL pulses using a velocity map imaging (VMI) detector that is sensitive to the polarization of light [38, 39]. We first acquired VMI images (projections of electron distributions onto a plane parallel to the propagation of the FEL beam) for pure linear horizontal and vertical polarizations L_H and L_V and assumed that for an arbitrary polarized FEL pulse (also the one in Fig. 2), the VMI image IM can be decomposed as their weighted sum $IM = a_H L_H + a_V L_V$, where $a_H, a_V \geq 0$ [40]. We then evaluated the difference-sum ratio $DSR = (a_H - a_V)/(a_H + a_V)$ as a function of the relative phase between the sub-pulses (it can be shown, that for energetic electrons and when the detector resolution is greater than the FEL pulse bandwidth, $DSR = \overline{S}_1/\overline{S}_0$, where $\overline{S}_1$ and $\overline{S}_0$ are the time-integrated Stokes parameters [33]).

The comparison between the experimental DSR and the one obtained by solving the time-dependent Schrödinger equation (TDSE) and projecting the photoelectron distributions onto the horizontal and vertical components [33] is shown in Fig. 3, bottom. For zero delay (left), the experimental DSR amplitude is less than the theoretical one (red curve), however, after including phase fluctuations at the same level ($\approx 0.06\lambda$) as for the co-rotating case, the theory (yellow curve) matches well with the experiment. For this cross-polarized configuration at zero delay, the maximum (minimum) signal at $\sim 0.1\lambda$ ($\sim 0.6\lambda$) corresponds to horizontal (vertical) polarization. As expected, the DSR amplitude is reduced for a 30 fs delay between the sub-pulses (right panel), partly due to a decreased overlap, but mainly due to additional fluctuations introduced by the delay undulator. Also here, after including the phase fluctuations at a level of $\approx 0.17\lambda$ (the same as for the co-rotating case), the theory agrees well with the experiment, demonstrating that the main factor that decreases the DSR amplitude are electron-beam energy fluctuations. For the 30 fs delay, the maximum (minimum) signal corresponds to horizontal (vertical) polarization in the overlap region ($t \sim 0$ fs).

The above results demonstrate the practical relevance of electron-beam energy/trajectory fluctuations, but also that they are at a level that will not compromise potential experiments, as shown by the non-vanishing DSR in the bottom right panel of Fig. 3. The phase stability, which becomes more critical at shorter FEL wavelengths, can be further increased by decreasing the FEL pulse duration (using a shorter seed), allowing a reduction of the sub-pulse delay (i.e., the strength of the dispersion; this will also preserve the microbunched structure in the electron beam even at short wavelengths) or by implementing the scheme at an FEL driven by a superconducting linear accelerator with lower shot-to-shot electron-beam energy fluctuations [41]. In addition, by monitoring the beam position in dispersive regions of the FEL line during the experiment, the data can be sorted with respect to the electron-beam energy in post-processing.

Because the contrast decreases with increasing sub-pulse delay, the results in Fig. 3 are direct evidence that we are indeed producing two delayed FEL pulses that will

generate the FEL output shown in Fig. 2 in the counter-rotating configuration. This method is valid for delays from 0 (theoretical $DSR = 1$) to no overlap ($DSR \sim 0$, delay $\sim$ 3×FWHM). To further investigate the pulse structure using a method with temporal resolution that is also valid for longer delays, we resorted to above-threshold ionization (ATI) in the presence of an optical dressing field. For this purpose, we spatially and temporally overlapped the FEL pulse with a short ($\sim$ 15 fs FWHM) and intense ($\sim 10^{13}$ W/cm^2) linearly polarized infrared (IR) laser ($\lambda \approx 800$ nm). The IR field gives rise to sidebands in the photoelectron spectra (separated by the IR photon energy), which correspond to additional absorption or stimulated emission of optical photons by the XUV-generated photoelectrons [42]. We acquired electrons from photoionization of He atoms as a function of the delay between the FEL and IR pulses using a magnetic bottle spectrometer (no angular resolution required this time) [43]. In such a cross-correlation experiment [42, 44], the IR probe pulse duration determines the length of the pulse structures that can still be resolved. For this set of experiments, the FEL sub-pulse duration estimated from the 70 fs seed duration [19, 34] and confirmed by cross-correlation measurements was 40 fs. Because our IR pulse was only $\sim 3\times$ shorter than the FEL sub-pulse, we analyzed the third sideband to reduce the effective probe pulse duration [34, 44] and increase the temporal resolution.

The cross-correlation measurements [33] for a delay between the FEL sub-pulse envelopes of 25 and 41 fs as a function of the relative phase between the sub-pulses are shown in the top and bottom left panels of Fig. 4, respectively. For the 25 fs delay, the photoelectron signal varies by changing the relative phase. In the center of the FEL pulse, the polarization is linear (see Fig. 2) and its direction rotates as a function of the phase, *i.e.*, it varies from being parallel to the IR polarization, where we observe the maximum photoionization (PE) yield, to being perpendicular to the IR polarization, where the minimum PE yield is observed. Such a variation of the photoelectron signal vs. the relative angle between the XUV and IR polarization vectors is expected based on angular momentum conservation rules [42].

Looking at the cross-correlation signal in the top left panel of Fig. 4, we see [33] that its shape can be described by two Gaussians separated by around 30 fs, which is close to the sub-pulse delay. For the 41 fs separation (bottom left panel), the variation of the PE yield vs. relative phase is observed again and is more restricted to the central part of the cross-correlation signal, where the pulse is linearly polarized. In this case, two peaks can be clearly resolved due to the increased separation (around 40 fs), which corresponds well to the sub-pulse delay.

The experimental PE yields agree well with the results of TDSE calculations [33] shown in the right panels of Fig. 4. The asymmetric shapes observed both in experiment and theory are due to the fact that the second sub-pulse is longer ($\sim$ 55 fs compared to 40 fs for the first

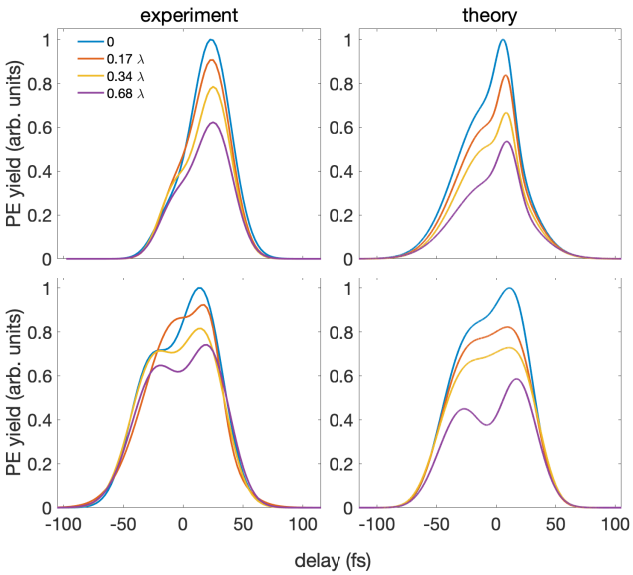

Figure 4: Experimental (left) and theoretical (right) total PE yields corresponding to the third sideband as a function of the delay between the FEL and IR pulses for different values of the relative phase between the FEL sub-pulses. The delay between the sub-pulse envelopes was 25 fs (top) and 41 fs (bottom).

sub-pulse), because the electron beam travels through the delay chicane [19, 34] - different sub-pulse durations have a negligible effect on the results in Fig. 3. A weaker variation of the PE yield vs. phase in the calculations compared to the experiment (especially for a 41 fs delay) is attributed to additional phase fluctuations introduced by the power supply of the magnetic chicane, which could not be measured on a shot-to-shot basis and were not included in the simulations (in Fig. 3, the delay was introduced using an undulator with permanent magnets). A more stable power supply, which we plan to implement in the future, will reduce the phase fluctuations.

Fig. 4 provides additional evidence that the two FEL sub-pulses are phase-locked, otherwise no variation of the PE yield vs. phase would be observed in the ATI experiments. Therefore, the fact that we have generated a linearly polarized pulse region, whose polarization direction depends on the phase shift between the FEL sub-pulses and whose extent (compared to the total FEL pulse duration) depends on the sub-pulse separation, together with the fact that we observe two peaks in the cross-correlation traces, can only mean that we have indeed generated two counter-rotating phase-locked sub-pulses that coherently add to form an FEL pulse with time-dependent polarization, such as the one shown in Fig. 2.

At this point we note that, if the counter-rotating pulses have slightly different wavelengths, additional polarization modulation (scrambling) will occur [45], which will modify the temporal structure shown in Fig. 2. However, for our set of electron-beam parameters (flat energy

profile) and operating wavelengths (tens of nm) the effect is negligible. On the other hand, imposing a controlled linear energy chirp onto the electron-beam profile can be used as an additional control parameter in experiments.

Improving energy resolution (e.g., employing a photon energy close to the ionization potential), we can directly test the predictions of generating electron vortices using single-photon photoionization in Ref. [46]. Applications in atomic and molecular physics also include coherent control of electron wave packets [47], and observing photoelectron circular dichroism within a single measurement [48]. Such experiments can now be performed without the need to prepare the target with additional pulses/and or the need to absorb many photons - the use of XUV pulses would involve different physics and shed new light on these measurements. In addition, our scheme is likely to find extensive application in dichroic spectroscopy of molecules [49–52], e.g., by varying the delay between pulses to extract chiral dynamics. The coherence between the pulses, absent in most of the cited references, permits the extraction of phase information if sufficiently high resolution is available (using a detector based on arrays of time-of-flight spectrometers). This work paves the way for even more sophisticated measurements, e.g., circularly polarized two-color experiments. It has already been shown at FERMI that two-color, linearly polarized light can be used for coherent control [53] and to extract the Wigner time for photoionization [54]. Photoelectron angular distributions have been calculated for overlapping, circularly polarized, two-color pulses [55] but a delay adds a further experimental control parameter. We envisage also applications in condensed matter, especially in the field of ultrafast magnetism, where it was recently shown [56–58] that magnetic dynamics (in particular when driven by the exchange interaction) may proceed on a femtosecond time scale. Having XUV sources generating polarization-shaped pulses on such time scales opens the door to pump-probe studies of coherent spin-dependent processes with element selectivity.

ACKNOWLEDGMENTS

This work was in part supported by the DFG (project no. 429194455). R.F. acknowledges financial support from the Swedish Research Council and the Knut and Alice Wallenberg Foundation, Sweden. The work of E.H. was supported by U.S. Department of Energy Award no. 2021-SLAC-100732. G.S. acknowledges financial support from the Deutsche Forschungsgemeinschaft Research Training Group DynCAM (RTG 2717) and grant 429805582 (project SA 3470/4-1). K.C.P. thanks Kenichi L. Ishikawa for helpful discussions. We acknowledge the support of the project "Structured light as a tool for triggering and probing new states of matter" (No. J1-3012), funded by the Slovenian Research Agency (ARRS).

[1] K. Misawa, Applications of polarization-shaped femtosecond laser pulses, Adv. in Phys. **1**, 544 (2016).
[2] H. Qi, Z. Lian, D. Fei, Z. Chen, and Z. Hu, Manipulation of matter with shaped-pulse light field and its applications, Adv.in Phys. **6**, 1949390 (2021).
[3] D. M. Villeneuve *et al.*, Forced molecular rotation in an optical centrifuge, Phys. Rev. Lett. **85**, 542 (2000).
[4] A. A. Milner *et al.*, Controlled enantioselective orientation of chiral molecules with an optical centrifuge, Phys. Rev. Lett. **122**, 223201 (2019).
[5] T. Brixner *et al.*, Quantum control by ultrafast polarization shaping, Phys. Rev. Lett. **92**, 208301 (2004).
[6] T. Suzuki, S. Minemoto, T. Kanai, and H. Sakai, Optimal control of multiphoton ionization processes in aligned $\mathbf{I_2}$ molecules with time-dependent polarization pulses, Phys. Rev. Lett. **92**, 133005 (2004).
[7] D. Pengel *et al.*, Electron vortices in femtosecond multiphoton ionization, Phys. Rev. Lett. **118**, 053003 (2017).
[8] K. Eickhoff *et al.*, Multichromatic polarization-controlled pulse sequences for coherent control of multiphoton ionization, Front. Phys. **9**, 675258 (2021).
[9] N. Dudovich *et al.*, Quantum control of the angular momentum distribution in multiphoton absorption processes, Phys. Rev. Lett. **92**, 103003 (2004).
[10] G. Sansone *et al.*, Isolated single-cycle attosecond pulses, Science **314**, 443 (2006).
[11] G. Sansone *et al.*, Shaping of attosecond pulses by phase-stabilized polarization gating, Phys. Rev. A **80**, 063837 (2009).
[12] N. Kanda *et al.*, The vectorial control of magnetization by light, Nat. Comm. **2**, 362 (2011).
[13] J. A. Myers, K. L. M. Lewis, P. F. Tekavec, and J. P. Ogilvie, Two-color two-dimensional fourier transform electronic spectroscopy with a pulse-shaper, Opt. Express **16**, 17420 (2008).
[14] S.-H. Shim and M. T. Zanni, How to turn your pump-probe instrument into a multidimensional spectrometer: 2d IR and Vis spectroscopies via pulse shaping, Phys. Chem. Chem. Phys. **11**, 737 (2009).
[15] T. Brixner and G. Gerber, Femtosecond polarization pulse shaping, Opt. Lett. **26**, 557 (2001).
[16] P. S. O. Masihzadeh and R. Bartels, Complete polarization state control of ultrafast laser pulses with a single linear spatial light modulator, Opt. Express **15**, 18025 (2007).
[17] T. S. M. Sato and K. Misawa, Interferometric polarization pulse shaper stabilized by an external laser diode for arbitrary vector field shaping, Rev. Sci. Instrum. **80**, 123107 (2009).
[18] E. Allaria *et al.*, Highly coherent and stable pulses from the FERMI seeded free-electron laser in the extreme ultraviolet, Nat. Photonics **6**, 699 (2012).
[19] D. Gauthier *et al.*, Spectrotemporal shaping of seeded free-electron laser pulses, Phys. Rev. Lett. **115**, 114801 (2015).
[20] D. Gauthier *et al.*, Generation of phase-locked pulses

from a seeded free-electron laser, Phys. Rev. Lett. **116**, 024801 (2016).
[21] N. S. Mirian *et al.*, Spectrotemporal control of soft x-ray laser pulses, Phys. Rev. Accel. Beams **23**, 060701 (2020).
[22] P. K. Maroju *et al.*, Attosecond pulse shaping using a seeded free-electron laser, Nature **578**, 386 (2020).
[23] O. Y. Gorobtsov *et al.*, Seeded x-ray free-electron laser generating radiation with laser statistical properties, Nat. Commun **9**, 4498 (2018).
[24] P. R. Ribič *et al.*, Coherent soft x-ray pulses from an echo-enabled harmonic generation free-electron laser, Nat. Photonics **13**, 555 (2019).
[25] G. Penco *et al.*, Nonlinear harmonics of a seeded free-electron laser as a coherent and ultrafast probe to investigate matter at the water window and beyond, Phys. Rev. A **105**, 053524 (2022).
[26] N. Sudar, R. Coffee, and E. Hemsing, Coherent x rays with tunable time-dependent polarization, Phys. Rev. Accel. Beams **23**, 120701 (2020).
[27] J. Morgan and B. W. J. McNeil, Attosecond polarization modulation of x-ray radiation in a free-electron laser, Phys. Rev. Accel. Beams **24**, 010701 (2021).
[28] J. Morgan and B. W. J. McNeil, X-ray pulse generation with ultra-fast flipping of its orbital angular momentum, Opt. Express **30**, 31171 (2022).
[29] E. Allaria *et al.*, Control of the polarization of a vacuum-ultraviolet, high-gain, free-electron laser, Phys. Rev. X **4**, 041040 (2014).
[30] E. Ferrari *et al.*, Free electron laser polarization control with interfering crossed polarized fields, Phys. Rev. Accel. Beams **22**, 080701 (2019).
[31] L. H. Yu, Generation of intense uv radiation by subharmonically seeded single-pass free-electron lasers, Phys. Rev. A **44**, 5178 (1991).
[32] The dispersion still has to be low enough to preserve the microbunched structure in the electron beam.
[33] See Supplemental Material at http://link.aps.org/supplemental/XXXX for details on FEL machine parameters, analysis of VMI images and cross-correlation measurements, and on the theoretical approach, which includes Refs. [59–63].
[34] P. Finetti *et al.*, Pulse duration of seeded free-electron lasers, Phys. Rev. X **7**, 021043 (2017).
[35] Note that the zero phase of PS is not calibrated and is different for all the plots, because the FEL required a reoptimization of operating parameters for each of the configurations.
[36] The uneven interval between points on the horizontal axis in the top panels is due to the fact that we performed the calibration of the current through the phase shifter vs. the phase after the measurements. On the other hand, the measurements in the bottom panels were performed with an already calibrated current step.
[37] 50 μm root mean square in both directions in the plane perpendicular to the beam propagation at each position monitor placed between the undulator sections.
[38] P. O'Keeffe *et al.*, A photoelectron velocity map imaging spectrometer for experiments combining synchrotron and laser radiations, Rev. Sci. Instrum. **82**, 033109 (2011).
[39] P. O'Keeffe *et al.*, A velocity map imaging apparatus for gas phase studies at FERMI@Elettra, Nucl. Instrum. Methods Phys. Res. B **284**, 69 (2012).
[40] S. T. Manson and A. F. Starace, Photoelectron angular distributions: energy dependence for *s* subshells, Rev. Mod. Phys. **54**, 389 (1982).
[41] W. Decking *et al.*, A MHz-repetition-rate hard x-ray free-electron laser driven by a superconducting linear accelerator, Nat. Photonics **14**, 391 (2020).
[42] M. Meyer *et al.*, Two-colour experiments in the gas phase, J. Phys. B: At. Mol. Opt. Phys. **43**, 194006 (2010).
[43] P. Kruit and F. H. Read, Magnetic field paralleliser for 2π electron-spectrometer and electron-image magnifier, J. Phys. E: Sci. Instrum. **16**, 313 (1983).
[44] A. Bouhal *et al.*, Cross-correlation measurement of femtosecond noncollinear high-order harmonics, J. Opt. Soc. Am. B **14**, 950 (1997).
[45] S. Serkez *et al.*, Method for polarization shaping at free-electron lasers, Phys. Rev. Accel. Beams **22**, 110705 (2019).
[46] J. M. N. Djiokap *et al.*, Electron vortices in photoionization by circularly polarized attosecond pulses, Phys. Rev. Lett. **115**, 113004 (2015).
[47] M. Wollenhaupt *et al.*, Interferences of ultrashort free electronwave packets, Phys. Rev. Lett. **89**, 173001 (2002).
[48] P. V. Demekhin *et al.*, Photoelectron circular dichroism with two overlapping laser pulses of carrier frequencies ω and 2ω linearly polarized in two mutually orthogonal directions, Phys. Rev. Lett. **121**, 253201 (2018).
[49] S. Beaulieu *et al.*, Attosecond-resolved photoionization of chiral molecules, Science **358**, 1288 (2017).
[50] S. Beaulieu *et al.*, Photoexcitation circular dichroism in chiral molecules, Nature Phys. **14**, 484 (2018).
[51] A. Comby *et al.*, Relaxation dynamics in photoexcited chiral molecules studied by time-resolved photoelectron circular dichroism: Toward chiral femtochemistry, J. Phys. Chem. Lett. **7**, 4514 (2016).
[52] S. Pan *et al.*, Manipulating parallel and perpendicular multiphoton transitions in H_2 molecules, Phys. Rev. Lett. **130**, 143203 (2023).
[53] K. C. Prince *et al.*, Coherent control with a short-wavelength free-electron laser, Nat. Photon. **10**, 176 (2016).
[54] D. You *et al.*, New method for measuring angle-resolved phases in photoemission, Phys. Rev. X **10**, 031070 (2020).
[55] E. V. Gryzlova *et al.*, Coherent control of the photoelectron angular distribution in ionization of neon by a circularly polarized bichromatic field in the resonance region, Phys. Rev. A **100**, 063417 (2019).
[56] F. Siegrist, J. A. Gessner, M. Ossiander, *et al.*, Light-wave dynamic control of magnetism, Nature **571**, 240 (2019).
[57] H. Hamamera, F. S. M. Guimarães, M. d. S. Dias, *et al.*, Polarisation-dependent single-pulse ultrafast optical switching of an elementary ferromagnet, Commun. Phys. **5**, 16 (2022).
[58] O. Neufeld, N. Tancogne-Dejean, U. D. Giovannini, *et al.*, Attosecond magnetization dynamics in non-magnetic materials driven by intense femtosecond lasers, npj Comput. Mater. **9**, 39 (2023).
[59] E. Allaria *et al.*, Two-stage seeded soft-x-ray free-electron laser, Nat. Photonics **7**, 913 (2013).
[60] A. T. J. B. Eppink and D. H. Parker, Velocity map imaging of ions and electrons using electrostatic lenses, Rev. Sci. Instrum. **68**, 3477 (1997).
[61] A. Sarsa, F. Gálvez, and E. Buendía, Parameterized optimized effective potential for the ground state of the atoms He through Xe, At. Data Nucl. Data Tables **88**, 163 (2004).

[62] M. Nurhuda and F. H. M. Faisal, Numerical solution of time-dependent Schrödinger equation for multiphoton processes: A matrix iterative method, Phys. Rev. A **60**, 3125 (1999).

[63] J. Laksman *et al.*, Commissioning of a photoelectron spectrometer for soft x-ray photon diagnostics at the european XFEL, J. Synchrotron. Radiat. **26**, 1010 (2019).